THE JOURNAL OF PHYSICAL CHEMISTRY Letters

Letter

Cite This: J. Phys. Chem. Lett. 2019, 10, 581−588

pubs.acs.org/JPCL

Unraveling the Metastability of C_n^{2+} (n = 2−4) Clusters

Zirong Peng,[†] David Zanuttini,[‡,§] Benoit Gervais,[*,§] Emmanuelle Jacquet,[§] Ivan Blum,[‡] Pyuck-Pa Choi,[†,∥] Dierk Raabe,[†] Francois Vurpillot,[‡] and Baptiste Gault[*,†]

[†]Department of Microstructure Physics and Alloy Design, Max-Planck-Institut für Eisenforschung GmbH, Max-Planck-Straße 1, 40237 Düsseldorf, Germany

[‡]Normandie Univ, UNIROUEN, INSA Rouen, CNRS, GPM, 76000 Rouen, France

[§]Normandie Univ, ENSICAEN, UNICAEN, CEA, CNRS, CIMAP, 14000 Caen, France

[∥]Department of Materials Science and Engineering, Korea Advanced Institute of Science and Technology (KAIST), 291 Daehak-ro, Yuseong-gu, Daejeon 305-338, Republic of Korea

Supporting Information

ABSTRACT: Pure carbon clusters have received considerable attention for a long time. However, fundamental questions, such as what the smallest stable carbon cluster dication is, remain unclear. We investigated the stability and fragmentation behavior of C_n^{2+} (n = 2−4) dications using state-of-the-art atom probe tomography. These small doubly charged carbon cluster ions were produced by laser-pulsed field evaporation from a tungsten carbide field emitter. Correlation analysis of the fragments detected in coincidence reveals that they only decay to C_{n-1}^{+} + C^{+}. During $C_2^{2+} \rightarrow C^{+} + C^{+}$, significant kinetic energy release (~5.75−7.8 eV) is evidenced. Through advanced experimental data processing combined with *ab initio* calculations and simulations, we show that the field-evaporated diatomic $^{12}C_2^{2+}$ dications are either in weakly bound $^3\Pi_u$ and $^3\Sigma_g^-$ states, quickly dissociating under the intense electric field, or in a deeply bound electronic $^5\Sigma_u^-$ state with lifetimes >180 ps.

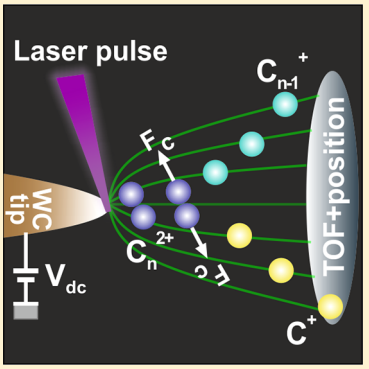

Since first detected in the tail of a comet in 1882,[1] pure carbon clusters have attracted considerable attention from physicists and chemists, which has translated into a vast amount of literature.[2−7] Carbon is one of the most abundant elements in the universe. Large to giant carbon clusters such as fullerenes, carbon nanotubes, and graphene are materials with rare combinations of mechanical and functional properties.[5,8−10] In turn, small carbon clusters play significant roles in combustion, astrophysics, and nuclear and plasma physics.[6,7,11] Besides their importance in numerous technological applications, carbon clusters are also highly valuable to basic theoretical research. C atoms can attain three different hybridizations, that is, sp, sp^2, and sp^3, which give rise to different types of C−C bonds and clusters with different structures, including linear chains, rings, 2D planes, 3D networks, and cages.[2] They provide a unique opportunity to gain deep insights into cluster structure and chemical bonding between atoms.

In 1933, L. Pauling discussed the stability of doubly charged helium dimer ions, He_2^{2+},[12] which has opened up a new perspective for understanding bonding and electronic properties of clusters. The stability of a charged cluster reflects the balance between the ionic Coulomb repulsion between the nuclei and the cohesion brought by the electrons. For a specific cluster, the amount of charge it can carry without being torn apart is limited. Similarly, for a particular charge state, only the clusters whose sizes are larger than a so-called *critical size* can resist Coulomb explosion.[13]

Owing to the strong covalent bond and extraordinary stability, fullerene ions C_{60}^{q+} have been studied the most extensively among the broad family of carbon clusters.[14] Much work has been done to determine the highest charge state that C_{60}^{q+} can reach before it becomes unstable. C_{60}^{2+} and C_{60}^{3+} were observed in the early 1990s.[15,16] Later, intact cations with q up to 7 and 10 were generated using electron impact[17] and ion impact[18,19] for ionization. C_{60}^{12+} produced by infrared radiation[20] is the most highly charged stable C_{60} cation reported so far. Theoretically, the Coulomb stability limit of C_{60}^{q+} was predicted to be q = 18[21,22] or q = 14[23−26] using a conducting sphere model or density functional theory (DFT).

In contrast, information on highly charged small carbon clusters is much scarcer. Fundamental questions, such as what the smallest stable carbon cluster dication is, remain unclear. Hogreve et al. performed a series of accurate multireference configuration interaction (MRCI) calculations on C_2^{2+},[27] C_3^{2+},[28] C_4^{2+},[29] and C_5^{2+}.[30] They found that C_2^{2+}, C_3^{2+}, and C_4^{2+} are all metastable in their lowest electronic state, and C_5^{2+} is the smallest carbon cluster ion exhibiting thermodynamic stability against charge separation.[30] Díaz-Tendero et al. reached the same conclusion by means of DFT and coupled-cluster (CC) theory simulations.[31] Wohrer et al. produced

Received: November 13, 2018
Accepted: January 23, 2019
Published: January 23, 2019

DOI: 10.1021/acs.jpclett.8b03449
J. Phys. Chem. Lett. 2019, 10, 581−588

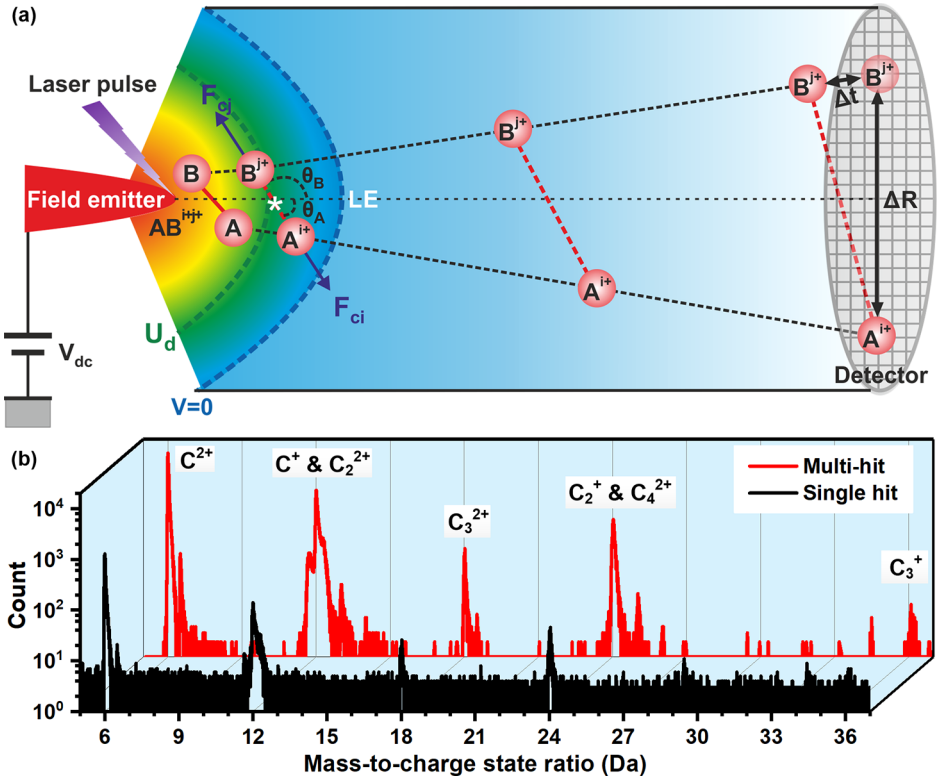

Figure 1. (a) Illustration of the experimental setup and a cluster ion fragmentation process. (b) Mass spectrum of carbon ions detected as single hits (black) or multihits (red) obtained from a cemented tungsten carbide sample.

both long-lived and excited C_5^{2+} ions by high-velocity collisions of 10 MeV C_5^+ ions with a He target.[32] They observed that conversely to metal cluster ions, whose dominant fission channels are those giving rise to almost symmetric fragments, the C_5^{2+} ions mainly decay to $C_4^+ + C^+$.[33] There is also experimental work reporting the detection of the C_n^{2+} (n = 2−4) cluster ions using time-of-flight (TOF) mass spectroscopy,[34,35] but the stability and fragmentation dynamics of the clusters have not been explored in detail.

Here we focus on the metastability of the three smallest carbon cluster dications, that is, C_n^{2+} n = (2−4). We conducted a detailed experimental investigation combined with *ab initio* calculations and simulations of the flight of ions from the emitter to the detector. Instead of using the above-mentioned conventional ionization methods, we applied laser-assisted field evaporation to produce C_2^{2+}, C_3^{2+}, and C_4^{2+} dications. Field evaporation is a process whereby the surface atoms of a field emitter, here a sharp needle of tungsten carbide, are desorbed and ionized under the effect of an intense electric field in the range of 10^{10} Vm^{-1}. Because the cluster ions are formed directly on the surface of the emitter upon desorption rather than by interaction with other energetic particles such as electrons, ions, and photons, the only source of their internal energy comes from the emission process itself. This is an advantage of our method.

The experiments were carried out using a straight-flight-path local electrode atom probe (CAMECA LEAP 5000 XS). Figure 1a illustrates the basic setup typically used for atom probe tomography (APT) experiments. The field emitter with a tip radius, r, <100 nm was held at a high positive voltage, V_{dc}, on the order of 3−10 kV in an ultrahigh vacuum chamber (10^{-10} to 10^{-11} mbar). As a result, a strong electrostatic field $F = \frac{V_{dc}}{rK_f}$ is created at the emitter surface. K_f is referred to as the geometrical field factor. It is mainly dependent on the shape of the field emitter and the electrostatic environment.[36,37] During experiments, V_{dc} was adjusted dynamically according to the current tip radius so that the strength of the electric field, F, was always slightly lower than that required for field evaporation. Subsequently, picosecond laser pulses were sent to the apex of the emitter to stimulate and time control the field evaporation process. Laser-pulsed field evaporation is a thermally activated process. After the interaction with the laser beam, the temperature of the emitter apex can increase up to a few hundred Kelvin.[38,39] High-temperature field evaporation leads to the appearance of cluster ions.[40] Then, it was rapidly cooled to the base temperature before the next laser pulse to prevent overheating and uncontrolled field evaporation under the electrostatic field alone. In our experiments, the base temperature of the emitter was set to 60 K. The time interval between the pulses was 4 μs, and the cooldown period of the emitter was estimated to be <6 ns based on the TOF spectrum. On the contrary, although the temperature elevation was relatively large, it only corresponded to a few vibrational numbers for C_2^{2+} and remained small with respect to the ground-state dissociation barrier of larger clusters, which is a favorable situation to study the Coulomb instability without possible bias induced by the large-amplitude vibrational motion and deformation associated with some excess internal energy. The local electrode (LE), placed ∼40 μm ahead of the emitting tip, was grounded to produce a well-defined, confined electric-field distribution near the emitter, which dropped rapidly toward the LE. By this electric field, the emitted ion was accelerated and projected onto a position-sensitive detector, where its TOF could be determined as the time period between the emission of the laser pulse and the

DOI: 10.1021/acs.jpclett.8b03449
J. Phys. Chem. Lett. 2019, 10, 581−588

moment the ion hit the time-resolved detector. The TOF was then converted into a mass-to-charge state ratio for elemental and isotopic identification. The detector used in the atom probe was a delay-line detector. It consisted of a stack of microchannel plates for signal amplification and three delay lines to enhance multihit detection capability,[41] that is, when more than one ion was generated by the same pulse. This multihit capability underpins the detection of the fragments from the dissociation of a cluster ion, and thus its complex decay dynamics can be determined by coincidence mapping. However, upon each ion impact, the propagation of signals along the delay lines causes a detector "dead time" and "dead zone", which could lead to the specific loss of certain ions. Consequently, the multihit was recorded as a single hit or the multiplicity of the hit, that is, the number of ions included in the multihit, would be underestimated. This issue is known as detector pile-up.[42] In another publication,[43] we closely studied the performance of the applied atom probe instrument on the multihit detection for C. The effects of the detector pile-up on this work are not critical.

Figure 1b shows experimental mass-to-charge state spectra of carbon ions detected as single hits (black) or in multihits (red) obtained from a tungsten carbide sample. In this experiment, we detected the multihits with a multiplicity up to 10. The relative occurrence frequency decreased with increasing multiplicity. 75.6% of them were double events, and 19.9% were triple events. Only <1% events had a multiplicity of 9 or 10. The multihit spectrum in Figure 1b contains carbon ions from all multihits, which are within either the C−C- or the C−W-type ion pairs. The C−W ion pairs, constituting 93.3%, are mainly formed due to correlated evaporation, that is, the sympathetic evaporation of adjacent atoms following the evaporation of a first atom.[44] The C−C ion pairs, constituting only 6.7%, are from either correlated evaporation or cluster dissociation, which we will discuss in this work. The relative contribution of cluster dissociation is small, but it can be easily separated from the nondissociative event because of the particular correlation on the mass-to-charge state ratios of the fragments.

Comparing the multihit spectrum with the single hit spectrum indicates that most of the carbon ions were detected as part of multihit events. This is common for the APT analysis of carbides[35] and is not limited to tungsten carbide. Carbon requires a high electric field for field evaporation, which may cause its retention on the emitter's surface and promote the formation of clusters.[45] Here we found atomic species, including C^+ and C^{2+}, and cluster species, including C_2^+, C_2^{2+}, C_3^+, C_3^{2+}, and C_4^{2+}. Because of the overlaps of the C^+ and C_2^+ peaks with the C_2^{2+} and C_4^{2+} peaks, respectively, it is difficult to estimate their relative abundances accurately from the mass spectrum itself, but their existence can be confirmed from the detailed correlation analysis of the multihit events. The known natural $^{12}C/^{13}C$ abundance ratio is 92.42.[46] In our measurement, the abundance ratios between the 6 and 6.5 Da peak are 90.56, 103.85, and 89.02 for overall, single, and multihit event mass spectra, respectively. As we discussed in another publication,[43] some $^{12}C^{2+}$−$^{12}C^{2+}$ multihits were incorrectly detected as single $^{12}C^{2+}$ hits when two $^{12}C^{2+}$ ions impacted the detector at nearly the same time and same position. Therefore, the $^{12}C^{2+}$ (6 Da)/$^{13}C^{2+}$ (6.5 Da) ratio measured in multihit and overall events is slightly lower than the natural abundance ratio, whereas for single-hit events, the opposite was observed. Besides, there is no clear indication of the formation of CH-type ions. Such species are frequently observed in APT analyses of organic samples[47,48] but are very rare in metal carbides.[35,49] If there was a substantial contribution of CH^{2+} to the 6.5 Da peak, then the abundance ratio of 6 Da/6.5 Da peak would be strongly shifted, which is, however, not the case.

Previously, Liu and Tsong also applied pulsed-laser-stimulated field evaporation and TOF mass spectroscopy to analyze carbon clusters. They observed carbon clusters consisting of up to 11 ions and showing a charge state of up to 3+.[34] Here we generated only small carbon clusters, arising from the distinctly different experimental conditions. We employed a tungsten carbide field emitter instead of graphite. Furthermore, Liu and Tsong applied a 337 nm wavelength, 50 μJ pulse energy, and 300 ps pulse width laser pulse, whereas we utilized a 355 nm wavelength, 120 pJ pulse energy, and ∼10 ps pulse width laser pulse. The increase in the temperature of the emitter is expected to be proportional to the peak power, which is five orders of magnitude smaller in our case. In addition, the position-sensitive detector has a good multihit capability, which allows us to register information about multiple fragments formed during the dissociation of a molecular ion. The differences in their TOF and hit positions can thus be analyzed to gain insights into the fragmentation process, especially the lifetime of the parent molecular ion.

Metastable cluster ions dissociate during their flight to the detector and give rise to multihits. The 12 and 24 Da peaks in the multihit mass spectrum are wider than those in the single hit mass spectrum. The C_3^+ peak is also more clearly visible. These are indications of cluster ion dissociation. In APT, the measured mass-to-charge state ratio of an ion, m', is calculated from its TOF value, t_f, using the equation $m' \propto 2eV_{dc}\left(\frac{t_f}{L}\right)^2$, where L is the length of the flight path (here ∼100 mm). For fragments resulting from in-flight dissociations of cluster ions, their TOF values and thus their measured mass-to-charge state ratios differ from their counterparts directly emitted from the emitter's surface. Consider, for example, the fragment A^{i+} from the dissociation process $AB^{i+j+} \rightarrow A^{i+} + B^{j+}$ sketched in Figure 1a. Following the assumption of instantaneous acceleration suggested by Saxey[50] and taking into account the kinetic energy release (KER) resulting from the fragment repulsion, we can deduce the measured mass-to-charge state ratio, m_A'

$$\frac{1}{m_A'} = \frac{\beta_d}{m_{AB}} + \frac{1-\beta_d}{m_A} + 2\cos\theta_A\sqrt{\frac{\beta_d}{m_{AB}}\frac{\gamma_A}{m_A}} \quad (1)$$

where m_A and m_{AB} are the true mass-to-charge state ratios of A^{i+} and AB^{i+j+}, respectively. $\beta_d = \frac{U-U_d}{U}$ $(0 \le \beta_d \le 1)$ describes the difference between the potential, U, at the emitter surface and the potential, U_d, at the position where the fragmentation takes place. The potential U_d is uniquely defined by the lifetime of the parent molecular ion, the applied voltage, and the initial conditions of the parent molecular ion, that is, its momentum and the position on the specimen's surface. θ_A is the angle between the Coulomb force, F_{ci}, and the local electric field generated by the tip. $\gamma_A = \frac{K_A}{2iU}$, where K_A is the KER provided to A^{i+}. A similar equation can also be obtained for fragment B^{j+}. We provide a detailed derivation of eq 1 in the Supporting Information (SI).

The deviations in mass-to-charge state ratio produce dissociation tracks in the multihit coincidence map[51] or,

DOI: 10.1021/acs.jpclett.8b03449
J. Phys. Chem. Lett. 2019, 10, 581−588

more specifically, ion-correlation histogram,[50] where the measured mass-to-charge state ratio of a hit is plotted against the measured mass-to-charge state ratio of another hit within the same multihit event. Figure 2 shows the ion-correlation histograms for C_2^{2+} (a), C_3^{2+} (b), and C_4^{2+} (c) dications. There is only one particular dissociation track for each species. With the help of eq 1, we can unambiguously identify the dissociation channels from the tracks, which are $C_2^{2+} \rightarrow C^+ + C^+$, $C_3^{2+} \rightarrow C^+ + C_2^+$, and $C_4^{2+} \rightarrow C^+ + C_3^+$ respectively. Previous theoretical work also indicates that the energetically favorable dissociation channel for these small carbon cluster dications C_n^{2+} (n = 2−5) is C_{n-1}^+/C^+,[27−30] and a previous experimental study on C_5^{2+} is in good agreement with this theoretical prediction.[33] Irrespective of the low detectability of neutrals in APT, tracks of dissociation channels that result in neutral fragments can also be identified using ion-correlation histograms.[52] Here dissociation channels with neutral fragment emission, that is, C_{n-1}^{2+}/C, C_{n-1}/C^{2+}, and C_{n-2}^{2+}/C_2, are not observed.

The red lines in Figure 2 are plotted according to

$$\frac{m_B'}{m_B} = \left(1 - \left(1 - \frac{m_A}{m_A'}\right)\frac{m_B - m_{AB}}{m_A - m_{AB}}\right)^{-1} \quad (2)$$

which is just eq 1 without the KER term and after elimination of the parametric β_d dependence. According to eq 1, three parameters play a role, namely, the magnitude of the KER itself, that is, K_A, the lifetime of the cluster ion, that is, β_d, and the orientation of the cluster ion, that is, θ_A. With the increase in the cluster ion lifetime, the impact of the KER becomes more and more distinct. For $C_3^{2+} \rightarrow C^+ + C_2^+$, the complete track aligns well with the red line, which is likely because the cluster axis is perpendicular to the electric field, that is, $\theta_A = \frac{\pi}{2}$, or the KER itself is small. For $C_4^{2+} \rightarrow C^+ + C_3^+$, we can observe a small offset near the point (m_{C_n}, m_{C_n}), that is, the place where the impact of the KER is expected to be most distinguishable. Both dissociation tracks of $C_3^{2+} \rightarrow C^+ + C_2^+$ and $C_4^{2+} \rightarrow C^+ + C_3^+$ are long, extending from the point of (m_{C_n}, m_{C_n}) to $(m_C, m_{C_{n-1}})$, but with higher intensity at the (m_{C_n}, m_{C_n}) extremity. This means that the majority of C_3^{2+} and C_4^{2+} ions dissociated relatively late; that is, their characteristic lifetimes are comparable to the TOF range of our spectrometer. The TOF is ∼400 ns for C_3^{2+} and ∼500 ns for C_4^{2+}, depending on the acceleration voltage. As a whole, the proportion of the C_3^{2+} and C_4^{2+} ions that dissociated is large, suggesting that the actual lifetimes of these species are significantly longer than the TOF and beyond the microsecond range. This is consistent with a previous observation of C_3^{2+} ions with TOF >20 μs.[34]

For homolytical dissociation of dications with an even number of carbon atoms such as C_2^{2+} and C_4^{2+}, that is, $C_{2n}^{2+} \rightarrow C_n^+ + C_n^+$, the true mass-to-charge state ratios of the two fragments, C_n^+ and the parent ion, C_{2n}^{2+}, are the same, and thus the KER is the only cause of a difference in the TOF, which translates into a difference in the measured mass-to-charge state ratio, Δm, between both fragments, giving rise to a dissociation track in the ion-correlation histogram. Because in this case $\theta_A + \theta_B = 180°$, that is, $\cos(\theta_A) = -\cos(\theta_B)$, we can eliminate the KER and angle dependence from eq 1 to get

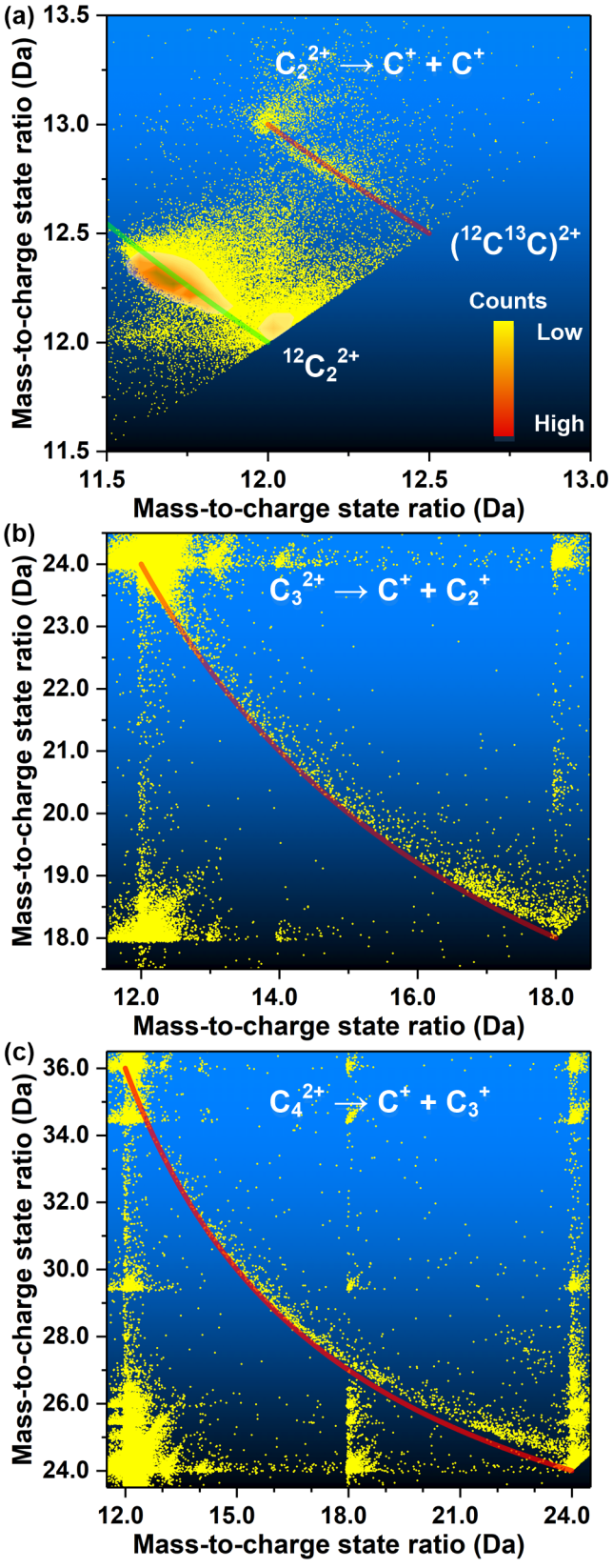

Figure 2. Cluster fragmentation tracks observed for (a) $C_2^{2+} \rightarrow C^+ + C^+$, (b) $C_3^{2+} \rightarrow C^+ + C_2^+$, and (c) $C_4^{2+} \rightarrow C^+ + C_3^+$. The green line in panel a corresponds to eq 3, and the red lines correspond to eq 2. In panel a, a color map indicating the intensity of the counts is included. The intensity of counts along the track is related to the time probability of dissociation, although not in an unequivocal bijective way.

DOI: 10.1021/acs.jpclett.8b03449
J. Phys. Chem. Lett. 2019, 10, 581−588

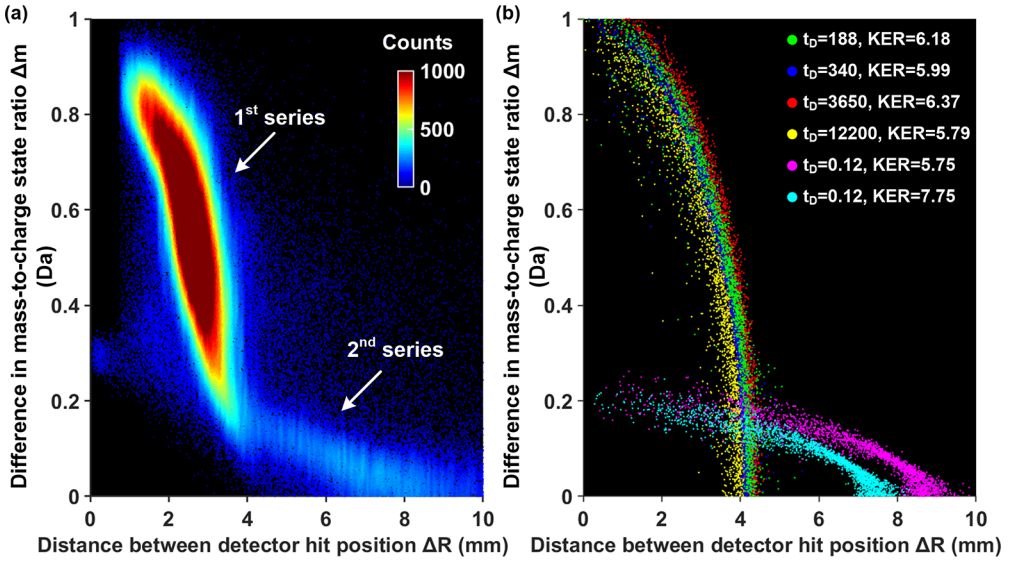

Figure 3. Plots showing the relationship between the differences in detector hit position and measured mass-to-charge state ratio of the two $^{12}C^+$ fragments of $^{12}C_2^{2+} \rightarrow {}^{12}C^+ + {}^{12}C^+$, obtained from (a) experiment and (b) simulation. In panel b, the results of the different dissociation time, t_D, that is, the lifetime of the cluster ions (in ps) and the kinetic energy release (KER) (in eV), are given. The dissociation distances corresponding to t_D are given in the SI.

$$m_A' = \frac{m_A}{2 - \frac{m_B}{m_B'}} \tag{3}$$

In Figure 2c, there is no obvious dissociation track corresponding to $C_4^{2+} \rightarrow C_2^+ + C_2^+$, either because the KER is too small to induce a noticeable difference in the measured mass-to-charge state ratio of the two C_2^+ fragments or simply because this type of dissociation is not energetically favorable and thus did not occur, as theoretically predicted.[29,31] In contrast, in Figure 2a, the dissociation track of $^{12}C_2^{2+} \rightarrow {}^{12}C^+ + {}^{12}C^+$ is very intense, implying a strong KER. The green line in this figure represents eq 3.

As Figure 1a illustrates, the KER induced by the repulsive Coulomb forces also causes divergences in the ion trajectories of the fragments (ΔR), which should negatively correlate with the difference in their measured mass-to-charge state ratios (Δm). The relationship observed for $^{12}C_2^{2+} \rightarrow {}^{12}C^+ + {}^{12}C^+$ is plotted in Figure 3a. Surprisingly, we can see two series of events. The first one leads to larger deviations in the measured mass-to-charge state ratio of fragments, whereas the second one results in larger distances between them. To better understand the dissociation process, we conducted a series of *ab initio* calculations to identify the bound states of $^{12}C_2^{2+}$ that are able to dissociate by means of intersystem crossing due to spin−orbit coupling (SOC). Our calculations to obtain the potential energy curves (PECs) closely follow the MRCI calculation by Hogreve.[27] According to these calculations, $^{12}C_2^{2+}$ has three metastable states, namely, $^5\Sigma_u^-$, $^3\Sigma_g^-$, and $^1\Delta_g$. The $^5\Sigma_u^-$ state has a deep potential energy well, with a large number of bound ro-vibrational states. Additional MRCI calculations taking into account a uniform static electric field show that the $^5\Sigma_u^-$ state is the only state able to resist the large electric field in the vicinity of the specimen's surface. Details of the MRCI calculations are summarized in the SI. An efficient fragmentation channel for the $^5\Sigma_u^-$ state is the intersystem crossing due to SOC with the $^3\Pi_u$ states. We have computed the lifetimes by means of perturbation theory using the method described in ref 53. In brief, the SOC lifetime for a given vibrational level is calculated from the vibrational wave function obtained from the MRCI potential energy curves and using a separate evaluation of the SOC matrix element, as described in the SI. Subsequently, we simulated the dissociation process of $^{12}C_2^{2+}$ along the $^3\Pi_u$ PEC using an idealized atom probe,[53,54] whose geometry is sketched in Figure 1a. Both the tip of the field emitter and the LE are mimicked using a confocal paraboloid following the method given in ref 53. The electric field at the tip apex was set at 46 V/nm, which is comparable to the electric fields applied in experiments.[55] The original $^{12}C_2^{2+}$ ions were randomly oriented with respect to the electric field. The distance between the two $^{12}C^+$ fragments at the dissociation time is taken in such a way that the potential energy on the $^3\Pi_u$ PEC equals the sum of the electronic and vibrational energies of the initial state for each vibrational state, $\nu = 0$−4.

Figure 3b shows the relationship between the measured mass-to-charge state ratio difference, Δm, of the two $^{12}C^+$ ions and their distance, ΔR, on the detector obtained from the simulations. For the first series of dissociation events, the lifetimes of $^{12}C_2^{2+}$ ions are governed by the intersystem crossing between the $^5\Sigma_u^-$ and $^3\Pi_u$ electronic state. The shortest lifetimes, linked to the lowest-energy vibrational states, are >180 ps, and the corresponding KER is >5.75 eV. The dissociation distance ranges from 6×10^4 to 4×10^6 nm for the dissociation times, t_D, included in Figure 3b. As Figure 3b demonstrates, the exact position of the dissociation track is insensitive to the lifetimes of the cluster ions but depends on the KER. As the KER increases with the vibrational number, ν, the impact distance, ΔR, on the detector progressively increases.

The second series of dissociation events observed in Figure 3a is well reproduced by a dissociation of the $^3\Sigma_g^-$ toward to the $^3\Pi_u$ states or a direct dissociation of the $^3\Pi_u$ state, with a distribution of KER ranging from 5.75 to 7.75 eV. The ground state $^3\Sigma_g^-$ has a long radiative lifetime by coupling with the $^3\Pi_u$ state.[27] However, the presence of the large electric field near the emitter's surface efficiently couples the $^3\Sigma_g^-$ state with the

DOI: 10.1021/acs.jpclett.8b03449
J. Phys. Chem. Lett. 2019, 10, 581−588

$^3\Pi_u$ state, leading to a quick dissociation in a time <1 ps. According to the postionization mechanism proposed by Kingham,[56] the $^{12}C_2^+$ ions are supposed to leave the surface of the emitter in their ground state, $^4\Sigma_g^-$, and then are ionized by electron tunneling to form one of the three lowest electronic states, that is, $^5\Sigma_u^-$, $^3\Pi_u$, and $^3\Sigma_g^-$. If the probabilities of removing electrons from different orbitals were the same, then statistically, the abundance ratio would be 5:6:3 for $^5\Sigma_u^-/^3\Pi_u/^3\Sigma_g^-$. This purely statistical ratio is not observed here, which may be due to the influence of the detector pile-up.[43] When the mass-to-charge state ratio difference of the successive $^{12}C_2^+$ ions in a multihit event is smaller than ∼0.3 Da, which is exactly the case of the second dissociation event, the detector will very likely only detect one of them. In addition, on the basis of Kingham's work,[56] the critical distance for ionization, where the postionization probability peaks, can be calculated. Using the work function of WC (3.6 eV)[57] and the ionization energy of C_2^+ (22.48 eV),[31] Kingham's theory predicts that all C_2^+ will be postionized into C_2^{2+} at an electrostatic field >14 V nm^{-1}. The time necessary to reach the critical distance at this field is in the range of 0.25 ps and could be considered as the lifetime of the C_2^+ ion. This result is remarkably consistent with the simulation hypothesis.

In summary, we demonstrated for the first time the metastability of the three smallest carbon cluster dications C_n^{2+} (n = 2−4) from both experiments as well as theoretical calculations and simulations. We evidenced that the energetically favorable dissociation channel for them is C_{n-1}^+/C^+. For the C_3^{2+} and C_4^{2+} species, we cannot obtain accurate lifetimes values from our experiments. The relatively large proportions of the nondissociated clusters suggest that their lifetimes extend beyond the microsecond range. For the C_2^{2+} ions, the experimental observation reveals that the tightly bound $^5\Sigma_u^-$ and the quickly dissociating $^3\Pi_u$ and $^3\Sigma_g^-$ electronic states are populated. The lifetime of the metastable $^5\Sigma_u^-$ state ranges from 0.2 to 12 ns depending on the vibrational state. The distinctly different lifetimes of the $^5\Sigma_u^-$, on the one hand, and of the $^3\Pi_u$ and $^3\Sigma_g^-$ states, on the other hand, lead to different degrees of divergence in their TOF and trajectories during APT analysis. These results support the postionization theory proposed by Kingham. The analysis reported here is not limited to tungsten carbide sample and small carbon cluster ions. Laser-assisted field evaporation can provide ready access to diverse types of molecular cations, which can already be noticed from literature. For instance, in the analysis of oxides,[58−62] carbides,[35,43,55] and nitrides,[50,52−54,63] oxygen, carbon, nitrogen, as well as (non)metal−oxygen, (non)metal−carbon, (non)metal−nitrogen cluster cations were observed. Large organic molecular ions were detected when measuring biological materials.[47,48] Combining this distinct strength with the time-resolved, position-sensitive detector equipped in APT opens a powerful way to study the stability and complex decay dynamics of multiply charged polyatomic ions.

■ ASSOCIATED CONTENT

Supporting Information

The Supporting Information is available free of charge on the ACS Publications website at DOI: 10.1021/acs.jpclett.8b03449.

1. Mathematical model of fragmentation tack. 2. Details of the *ab initio* calculation (PDF)

■ AUTHOR INFORMATION

Corresponding Authors

*E-mail: gervais@ganil.fr (B. Gervais).
*E-mail: b.gault@mpie.de (B. Gault).

ORCID

Zirong Peng: 0000-0001-7844-8313
Benoit Gervais: 0000-0003-0707-550X
Ivan Blum: 0000-0002-4729-6510

Notes

The authors declare no competing financial interest.

■ ACKNOWLEDGMENTS

We are grateful to Uwe Tezins and Andreas Sturm for their support of the APT, SEM, and FIB facilities at Max-Planck-Institut für Eisenforschung GmbH. Z.P. and B.G. are grateful to Dr. Michael Ashton from the University of Florida, Gainesville (now in MPIE) and Prof. Susan Sinnott from Penn State University for preliminary discussions and results on the dissociation energies of cluster ions. This work was supported financially by the EMC3 LabEx, AQURATE project, and BigMax project (Big-data-driven materials science https://www.bigmax.mpg.de/).

■ REFERENCES

(1) Huggins, W. Preliminary Note on the Photographic Spectrum of Comet b 1881. *Proc. R. Soc. London* **1882**, *33*, 1−3.
(2) Inagaki, M.; Kang, F. *Materials Science and Engineering of Carbon: Fundamentals*, 2nd ed.; Butterworth-Heinemann: Oxford, U.K., 2014.
(3) Lifshitz, C. Carbon Clusters. *Int. J. Mass Spectrom.* **2000**, *200*, 423−442.
(4) Varandas, A. J. C.; Rocha, C. M. R. Cn(N = 2−4): Current Status. *Philos. Trans. R. Soc., A* **2018**, *376*, 1−46.
(5) Georgakilas, V.; Perman, J. A.; Tucek, J.; Zboril, R. Broad Family of Carbon Nanoallotropes: Classification, Chemistry, and Applications of Fullerenes, Carbon Dots, Nanotubes, Graphene, Nanodiamonds, and Combined Superstructures. *Chem. Rev.* **2015**, *115*, 4744−4822.
(6) Van Orden, A.; Saykally, R. J. Small Carbon Clusters: Spectroscopy, Structure, and Energetics. *Chem. Rev.* **1998**, *98*, 2313−2358.
(7) Weltner, W.; Van Zee, R. J. Carbon Molecules, Ions, and Clusters. *Chem. Rev.* **1989**, *89*, 1713−1747.
(8) Kroto, H. W.; Heath, J. R.; O'Brien, S. C.; Curl, R. F.; Smalley, R. E. C60: Buckminsterfullerene. *Nature* **1985**, *318*, 162−163.
(9) Dresselhaus, M. S.; Dresselhaus, G.; Eklund, P. C. *Science of Fullerenes and Carbon Nanotubes*; Academic Press, 1996.
(10) Thostenson, E. T.; Ren, Z.; Chou, T.-W. Advances in the Science and Technology of Carbon Nanotubes and Their Composites: A Review. *Compos. Sci. Technol.* **2001**, *61*, 1899−1912.
(11) *Combustion Chemistry*; Gardiner, W. C., Ed.; Springer US: New York, 1984.
(12) Pauling, L. The Normal State of the Helium Molecule-Ions He_2^+ and He_2^{+2}. *J. Chem. Phys.* **1933**, *1*, 56−59.
(13) *Clusters of Atoms and Molecules: Theory, Experiment, and Clusters of Atoms*; Haberland, H., Ed.; Springer Series in Chemical Physics; Springer, 1994; Vol. 52.
(14) Echt, O.; Scheier, P.; Märk, T. D. Multiply Charged Clusters. *C. R. Phys.* **2002**, *3*, 353−364.
(15) Steger, H.; de Vries, J.; Kamke, B.; Kamke, W.; Drewello, T. Direct Double Ionization of C_{60} and C_{70} Fullerenes Using Synchrotron Radiation. *Chem. Phys. Lett.* **1992**, *194*, 452−456.
(16) Böhme, D. K. Fullerene Ion Chemistry: A Journey of Discovery and Achievement. *Philos. Trans. R. Soc., A* **2016**, *374*, 1−16.

DOI: 10.1021/acs.jpclett.8b03449
J. Phys. Chem. Lett. 2019, 10, 581−588

(17) Scheier, P.; Märk, T. D. Observation of the Septuply Charged Ion C_{60}^{7+} and Its Metastable Decay into Two Charged Fragments via Superasymmetric Fission. *Phys. Rev. Lett.* **1994**, *73*, 54−57.
(18) Jin, J.; Khemliche, H.; Prior, M. H.; Xie, Z. New Highly Charged Fullerene Ions: Production and Fragmentation by Slow Ion Impact. *Phys. Rev. A: At., Mol., Opt. Phys.* **1996**, *53*, 615−618.
(19) Brenac, A.; Chandezon, F.; Lebius, H.; Pesnelle, A.; Tomita, S.; Huber, B. A. Multifragmentation of Highly Charged C_{60} Ions: Charge States and Fragment Energies. *Phys. Scr.* **1999**, *T80*, 195−196.
(20) Bhardwaj, V. R.; Corkum, P. B.; Rayner, D. M. Internal Laser-Induced Dipole Force at Work in C_{60} Molecule. *Phys. Rev. Lett.* **2003**, *91*, 203004.
(21) Zettergren, H.; Schmidt, H. T.; Cederquist, H.; Jensen, J.; Tomita, S.; Hvelplund, P.; Lebius, H.; Huber, B. A. Static Over-the-Barrier Model for Electron Transfer between Metallic Spherical Objects. *Phys. Rev. A: At., Mol., Opt. Phys.* **2002**, *66*, 32710.
(22) Zettergren, H.; Jensen, J.; Schmidt, H. T.; Cederquist, H. Electrostatic Model Calculations of Fission Barriers for Fullerene Ions. *Eur. Phys. J. D* **2004**, *29*, 63−68.
(23) Díaz-Tendero, S.; Alcamí, M.; Martín, F. Coulomb Stability Limit of Highly Charged C_{60}^{Q+} Fullerenes. *Phys. Rev. Lett.* **2005**, *95*, 13401.
(24) Díaz-Tendero, S.; Alcamí, M.; Martín, F. Structure and Electronic Properties of Highly Charged C_{60} and C_{58} Fullerenes. *J. Chem. Phys.* **2005**, *123*, 184306.
(25) Sahnoun, R.; Nakai, K.; Sato, Y.; Kono, H.; Fujimura, Y.; Tanaka, M. Theoretical Investigation of the Stability of Highly Charged C_{60} Molecules Produced with Intense near-Infrared Laser Pulses. *J. Chem. Phys.* **2006**, *125*, 184306.
(26) Sahnoun, R.; Nakai, K.; Sato, Y.; Kono, H.; Fujimura, Y.; Tanaka, M. Stability Limit of Highly Charged C_{60} Cations Produced with an Intense Long-Wavelength Laser Pulse: Calculation of Electronic Structures by DFT and Wavepacket Simulation. *Chem. Phys. Lett.* **2006**, *430*, 167−172.
(27) Hogreve, H. Theoretical Study of the Low-Lying Electronic Spectrum of C_2^{2+}. *Chem. Phys.* **1996**, *202*, 63−80.
(28) Hogreve, H. Ab Initio Study of the Dication Carbon Trimer C_3^{2+}. *J. Chem. Phys.* **1995**, *102*, 3281−3291.
(29) Hogreve, H. Stability Properties of C_4^{2+}. *J. Mol. Struct.: THEOCHEM* **2000**, *532*, 81−86.
(30) Hogreve, H.; Jalbout, A. F. The Carbon Pentamer Dication C_5^{2+}: Toward Thermochemical Stability. *J. Chem. Phys.* **2003**, *119*, 8849−8853.
(31) Díaz-Tendero, S.; Martín, F.; Alcamí, M. Structure, Dissociation Energies, and Harmonic Frequencies of Small Doubly Charged Carbon Clusters C_n^{2+} (n = 3−9). *J. Phys. Chem. A* **2002**, *106*, 10782−10789.
(32) Wohrer, K.; Chabot, M.; Rozet, J. P.; Gardès, D.; Vernhet, D.; Jacquet, D.; Negra, S. D.; Brunelle, A.; Nectoux, M.; Pautrat, M.; et al. Swift Cluster-Atom Collisions: Experiment and Model Calculations. *J. Phys. B: At., Mol. Opt. Phys.* **1996**, *29*, L755−L761.
(33) Chabot, M.; Wohrer, K.; Rozet, J. P.; Gardès, D.; Vernhet, D.; Jacquet, D.; Negra, S. D.; Brunelle, A.; Nectoux, M.; Pautrat, M.; et al. Fragmentation Patterns of Ionized C_5^{Q+} Clusters (Q = 1 → 4). *Phys. Scr.* **1997**, *T73*, 282−283.
(34) Liu, J.; Tsong, T. T. Kinetic-Energy and Mass Analysis of Carbon Cluster Ions in Pulsed-Laser-Stimulated Field Evaporation. *Phys. Rev. B: Condens. Matter Mater. Phys.* **1988**, *38*, 8490−8493.
(35) Thuvander, M.; Weidow, J.; Angseryd, J.; Falk, L. K. L.; Liu, F.; Sonestedt, M.; Stiller, K.; Andrén, H.-O. Quantitative Atom Probe Analysis of Carbides. *Ultramicroscopy* **2011**, *111*, 604−608.
(36) Gomer, R. *Field Emission and Field Ionization*; Harvard University Press: Cambridge, U.K., 1961.
(37) Loi, S. T.; Gault, B.; Ringer, S. P.; Larson, D. J.; Geiser, B. P. Electrostatic Simulations of a Local Electrode Atom Probe: The Dependence of Tomographic Reconstruction Parameters on Specimen and Microscope Geometry. *Ultramicroscopy* **2013**, *132*, 107−113.
(38) Kellogg, G. L.; Tsong, T. T. Pulsed-Laser Atom-Probe Field-Ion Microscopy. *J. Appl. Phys.* **1980**, *51*, 1184−1193.
(39) Diercks, D. R.; Gorman, B. P. Nanoscale Measurement of Laser-Induced Temperature Rise and Field Evaporation Effects in CdTe and GaN. *J. Phys. Chem. C* **2015**, *119*, 20623−20631.
(40) Tsong, T. T.; Liou, Y. Cluster-Ion Formation in Pulsed-Laser-Stimulated Field Desorption of Condensed Materials. *Phys. Rev. B: Condens. Matter Mater. Phys.* **1985**, *32*, 4340−4357.
(41) Da Costa, G.; Vurpillot, F.; Bostel, A.; Bouet, M.; Deconihout, B. Design of a Delay-Line Position-Sensitive Detector with Improved Performance. *Rev. Sci. Instrum.* **2005**, *76*, No. 013304.
(42) Da Costa, G.; Wang, H.; Duguay, S.; Bostel, A.; Blavette, D.; Deconihout, B. Advance in Multi-Hit Detection and Quantization in Atom Probe Tomography. *Rev. Sci. Instrum.* **2012**, *83*, 123709.
(43) Peng, Z.; Vurpillot, F.; Choi, P.-P. P.; Li, Y.; Raabe, D.; Gault, B. On the Detection of Multiple Events in Atom Probe Tomography. *Ultramicroscopy* **2018**, *189*, 54−60.
(44) De Geuser, F.; Gault, B.; Bostel, A.; Vurpillot, F. Correlated Field Evaporation as Seen by Atom Probe Tomography. *Surf. Sci.* **2007**, *601*, 536−543.
(45) Gault, B.; Danoix, F.; Hoummada, K.; Mangelinck, D.; Leitner, H. Impact of Directional Walk on Atom Probe Microanalysis. *Ultramicroscopy* **2012**, *113*, 182−191.
(46) de Laeter, J. R.; Böhlke, J. K.; De Bièvre, P.; Hidaka, H.; Peiser, H. S.; Rosman, K. J. R.; Taylor, P. D. P. Atomic Weights of the Elements. Review 2000. *Pure Appl. Chem.* **2003**, *75*, 683−800.
(47) Nishikawa, O.; Taniguchi, M. Scanning Atom-Probe Analysis of Carbon-Based Materials. *19th Int. Vac. Nanoelectron. Conf.* **2006**, 67−68.
(48) Taniguchi, M.; Nishikawa, O. Atomic Level Analysis of Dipeptide Biomolecules by a Scanning Atom Probe. *J. Vac. Sci. Technol., B: Nanotechnol. Microelectron.: Mater., Process., Meas., Phenom.* **2016**, *34*, No. 03H109.
(49) Sha, W.; Chang, L.; Smith, G. D. W.; Liu, C.; Mittemeijer, E. J. Some Aspects of Atom-Probe Analysis of Fe-C and Fe-N Systems. *Surf. Sci.* **1992**, *266*, 416−423.
(50) Saxey, D. W. Correlated Ion Analysis and the Interpretation of Atom Probe Mass Spectra. *Ultramicroscopy* **2011**, *111*, 473−479.
(51) Eland, J. H. D. A New Two-Parameter Mass Spectrometry. *Acc. Chem. Res.* **1989**, *22*, 381−387.
(52) Gault, B.; Saxey, D. W.; Ashton, M. W.; Sinnott, S. B.; Chiaramonti, A. N.; Moody, M. P.; Schreiber, D. K. Behavior of Molecules and Molecular Ions near a Field Emitter. *New J. Phys.* **2016**, *18*, No. 033031.
(53) Zanuttini, D.; Vurpillot, F.; Douady, J.; Jacquet, E.; Anglade, P.-M.; Gervais, B. Dissociation of GaN^{2+} and AlN^{2+} in APT: Electronic Structure and Stability in Strong DC Field. *J. Chem. Phys.* **2018**, *149*, 134310.
(54) Zanuttini, D.; Blum, I.; di Russo, E.; Rigutti, L.; Vurpillot, F.; Douady, J.; Jacquet, E.; Anglade, P.-M.; Gervais, B. Dissociation of GaN^{2+} and AlN^{2+} in APT: Analysis of Experimental Measurements. *J. Chem. Phys.* **2018**, *149*, 134311.
(55) Peng, Z.; Choi, P.-P.; Gault, B.; Raabe, D. Evaluation of Analysis Conditions for Laser-Pulsed Atom Probe Tomography: Example of Cemented Tungsten Carbide. *Microsc. Microanal.* **2017**, *23*, 431−442.
(56) Kingham, D. R. The Post-Ionization of Field Evaporated Ions: A Theoretical Explanation of Multiple Charge States. *Surf. Sci.* **1982**, *116*, 273−301.
(57) Fomenko, V. S. *Handbook of Thermionic Properties: Electronic Work Functions and Richardson Constants of Elements and Compounds*; Samsonov, G. V., Ed.; Plenum Press Data Division: New York, 1966.
(58) Peng, Z.; Rohwerder, M.; Choi, P.-P.; Gault, B.; Meiners, T.; Friedrichs, M.; Kreilkamp, H.; Klocke, F.; Raabe, D. Atomic Diffusion Induced Degradation in Bimetallic Layer Coated Cemented Tungsten Carbide. *Corros. Sci.* **2017**, *120*, 1−13.
(59) Santhanagopalan, D.; Schreiber, D. K.; Perea, D. E.; Martens, R. L.; Janssen, Y.; Khalifah, P.; Meng, Y. S. Effects of Laser Energy and

DOI: 10.1021/acs.jpclett.8b03449
J. Phys. Chem. Lett. 2019, 10, 581−588

Wavelength on the Analysis of $LiFePO_4$ Using Laser Assisted Atom Probe Tomography. *Ultramicroscopy* **2015**, *148*, 57−66.
(60) Zanuttini, D.; Blum, I.; Rigutti, L.; Vurpillot, F.; Douady, J.; Jacquet, E.; Anglade, P.-M.; Gervais, B. Simulation of Field-Induced Molecular Dissociation in Atom-Probe Tomography: Identification of a Neutral Emission Channel. *Phys. Rev. A: At., Mol., Opt. Phys.* **2017**, *95*, No. 061401.
(61) Devaraj, A.; Colby, R.; Hess, W. P.; Perea, D. E.; Thevuthasan, S. Role of Photoexcitation and Field Ionization in the Measurement of Accurate Oxide Stoichiometry by Laser-Assisted Atom Probe Tomography. *J. Phys. Chem. Lett.* **2013**, *4*, 993−998.
(62) Blum, I.; Rigutti, L.; Vurpillot, F.; Vella, A.; Gaillard, A.; Deconihout, B. Dissociation Dynamics of Molecular Ions in High Dc Electric Field. *J. Phys. Chem. A* **2016**, *120*, 3654−3662.
(63) Riley, J. R.; Bernal, R. A.; Li, Q.; Espinosa, H. D.; Wang, G. T.; Lauhon, L. J. Atom Probe Tomography of A-Axis GaN Nanowires: Analysis of Nonstoichiometric Evaporation Behavior. *ACS Nano* **2012**, *6*, 3898−3906.

DOI: 10.1021/acs.jpclett.8b03449
J. Phys. Chem. Lett. 2019, 10, 581−588